

This is the accepted manuscript made available via CHORUS. The article has been published as:

Observation of the magnetic  $C_{\{4\}}$  phase in  $\text{Ca}_{\{1-x\}}\text{Na}_{\{x\}}\text{Fe}_{\{2\}}\text{As}_{\{2\}}$  and its universality in the hole-doped 122 superconductors

K. M. Taddei, J. M. Allred, D. E. Bugaris, S. H. Lapidus, M. J. Krogstad, H. Claus, D. Y. Chung, M. G. Kanatzidis, R. Osborn, S. Rosenkranz, and O. Chmaissem

Phys. Rev. B **95**, 064508 — Published 15 February 2017

DOI: [10.1103/PhysRevB.95.064508](https://doi.org/10.1103/PhysRevB.95.064508)

# Observation of the magnetic $C_4$ phase in $\text{Ca}_{1-x}\text{Na}_x\text{Fe}_2\text{As}_2$ and its universality in the hole-doped 122 superconductors

K.M. Taddei,<sup>1,2,3,\*</sup> J.M. Allred,<sup>3</sup> D.E. Bugaris,<sup>3</sup> S. Lapidus,<sup>4</sup> M. Krogstad,<sup>2,3</sup> H. Claus,<sup>3</sup>  
D.Y. Chung,<sup>3</sup> M. Kanatzidis,<sup>3,5</sup> R. Osborn,<sup>3</sup> S. Rosenkranz,<sup>3</sup> and O. Chmaissem<sup>2,3</sup>

<sup>1</sup>*Quantum Condensed Matter Division, Oak Ridge National Laboratory, Oak Ridge, TN, 37831, USA*

<sup>2</sup>*Department of Physics, Northern Illinois University, DeKalb, IL 60115, USA*

<sup>3</sup>*Materials Science Division, Argonne National Laboratory, Argonne, IL 60439, USA*

<sup>4</sup>*Advanced Photon Source, Argonne National Laboratory, Argonne, IL 60439, USA*

<sup>5</sup>*Department of Chemistry, Northwestern University, Evanston, IL 60208, USA*

(Dated: January 25, 2017)

Since its discovery in 2014 the magnetic tetragonal  $C_4$  phase has been identified in a growing number of hole-doped ‘122’ Fe-based superconducting compounds. Exhibiting a unique double- $\mathbf{Q}$  magnetic structure and a strong competition with both superconducting and magnetic order parameters, the  $C_4$  phase and the conditions of its formation are of significant interest to understanding the fundamental mechanisms in these materials. Particularly, separating the importance of direct changes to the relative size of hole and electron pockets at the Fermi surface (achieved via charge doping) from the role of structural changes due to differences of ionic radii of dopants is useful to determine the underlying parameter which causes the  $C_4$  instability. Here, we report the discovery of the  $C_4$  phase in a fourth member of the hole-doped ‘122’ materials  $\text{Ca}_{1-x}\text{Na}_x\text{Fe}_2\text{As}_2$  ( $0.20 \leq x \leq 0.50$ ) as determined from neutron and X-ray powder diffraction studies. The maximum of the  $C_4$  dome is observed at  $x = 0.44$  with a re-entrant temperature  $T_r = 52\text{K}$  and an extent of  $\Delta x \sim 0.07$  in composition. It is observed that for a range of compositions within the  $C_4$  dome ( $0.40 \leq x \leq 0.42$ ) there is a second re-entrance ( $T_{r2} < T_r$ ) where the AFM- $C_2$  phase is recovered - a feature previously only seen in  $\text{Ba}_{1-x}\text{K}_x\text{Fe}_2\text{As}_2$ . A phase diagram is presented for  $\text{Ca}_{1-x}\text{Na}_x\text{Fe}_2\text{As}_2$  and compared to the other  $\text{Na}^+$ -doped ‘122’s’ -  $\text{A}_{1-x}\text{Na}_x\text{Fe}_2\text{As}_2$  with  $\text{A} = \text{Ba}, \text{Sr}$  and  $\text{Ca}$ . The structural parameters for these three systems are compared and the importance of the ‘chemical pressure’ due to changing the  $\text{A}$ -site ion ( $\text{A} = \text{Ba}, \text{Sr}, \text{Ca}$ ) is discussed.

PACS numbers: 74.25.Dw, 74.62.Dh, 74.70.Xa, 61.05.fm

## I. INTRODUCTION

There has been a debate about the Fe-based superconductors (FBS) over whether a spin/itinerant or localized orbital treatment is the appropriate model for their electronic behavior since their discovery in 2006.<sup>1</sup> Despite similarities to the well-studied cuprate superconductors which might suggest a localized picture, behaviors such as ‘poor-metal’ properties (rather than Mott-insulating), Fermi surface (FS) nesting driven spin-density wave (SDW) magnetic ordering and strong magneto-elastic coupling indicate the importance of itinerant spin dynamics in correctly describing these systems.<sup>2–5</sup> Indeed, measurements of different properties have found support of either model with magnetic torque, resistivity anisotropy and orbital ordering supporting orbital mechanics while measurements of the dynamic spin excitations, strain magnetism coupling and magnetoelastic scaling strongly suggesting a spin-driven scenario.<sup>6–11</sup> Yet determining the correct model, and consequently the underlying primary order parameter, is vital to understanding the mechanism of superconductivity in these systems. The recent discovery of a new magnetic phase with fourfold  $C_4$  symmetry in the hole-doped ‘122’ FBS evidenced the vital role of itinerant electronic behavior in determining the behavior of these materials. Furthermore, it has opened up a new avenue to study the inter-

play of magnetism and superconductivity.<sup>12,13</sup>

The  $C_4$  phase has been observed in three members of the hole-doped ‘122’ family so far:  $\text{Ba}_{1-x}\text{Na}_x\text{Fe}_2\text{As}_2$ ,  $\text{Ba}_{1-x}\text{K}_x\text{Fe}_2\text{As}_2$  and most recently  $\text{Sr}_{1-x}\text{Na}_x\text{Fe}_2\text{As}_2$ .<sup>12–14</sup> In these materials the typical suppression of the antiferromagnetically (AFM) ordered orthorhombic  $C_2$  phase (so-called for the 2-fold rotation axis) upon doping is complicated by a re-entrant tetragonal ( $I4/mmm$  symmetry) magnetically re-orientated  $C_4$  phase. This higher symmetry phase appears at temperatures ( $T_r$ ) below the  $C_2$  transition ( $T_N$ ) and at compositions ( $x$ ) less than or equal to the critical concentration ( $x_c$ ) beyond which no ordered magnetism is observed. This describes a  $C_4$  dome which exists near the complete suppression of the  $C_2$  dome.

The  $C_4$  phase inhabits a unique intersection, exhibiting not only an exotic magnetic double- $\mathbf{Q}$  structure born of the superposition of two itinerant SDW’s but also forming in the vicinity of superconductivity. Consequently, it has become the focus of many recent first principle reports to reveal what parameters are causing the sudden reordering of the single- $\mathbf{Q}$   $C_2$  structure into this novel double- $\mathbf{Q}$  structure and how this new phase hosts superconductivity.<sup>12,15–19</sup> Currently, several different proposed models predict the observed  $C_4$  but they do so through different mechanisms which range from expanded itinerant mean field models to impurity

scattering stabilization to spin-orbit coupling driven spin anisotropies.<sup>15,17,18</sup> The different models invoke varying assumptions about the underlying physics in these materials and necessarily predict different, sometimes subtly so, manifestations of the  $C_4$  phase. It is therefore worthwhile to attempt to discern between these models in order to inform future investigations. While some of the subtler new predictions made are experimentally challenging to verify one relatively simple validation is comparison of the predicted phase diagrams with those found experimentally - specifically in the manifestation in temperature and composition space of the  $C_4$  phase and its competition with superconductivity and the  $C_2$  magnetic ordering. Such comparisons help not only in discerning between different models but also in designating possible physically realized ranges of parameters within each model.

It is therefore, relevant to return to previously studied hole-doped ‘122’s’ to search for the presence of the  $C_4$  phase, whose small extent in composition is easy to miss in less exhaustive work. Such studies have so far found  $C_4$  in both the well-studied  $\text{Ba}_{1-x}\text{K}_x\text{Fe}_2\text{As}_2$  and  $\text{Sr}_{1-x}\text{Na}_x\text{Fe}_2\text{As}_2$  materials.<sup>14,20</sup> The robust  $C_4$  phase found in this latter system informs a return to the  $\text{Na}^+$  doped  $\text{CaFe}_2\text{As}_2$ . Several reported phase diagrams for  $\text{Ca}_{1-x}\text{Na}_x\text{Fe}_2\text{As}_2$  exist notably in References 21 and 22 however, their authors’ use of large steps in composition mean that any  $C_4$  phase would likely have been missed. Furthermore, thus far no clear evidence of the  $C_4$  phase has been reported from either magnetization or resistivity measurements indicating that even with the right compositions the phase can be missed in the absence of temperature dependent diffraction studies. Therefore, the large number of studies on  $\text{Ca}_{1-x}\text{Na}_x\text{Fe}_2\text{As}_2$  which have relied on these characterization techniques would not necessarily have been sensitive to this phase re-entrance.<sup>23–26</sup>

In this paper we determine the  $\text{Ca}_{1-x}\text{Na}_x\text{Fe}_2\text{As}_2$  phase diagram and present the results of a careful systematic structural and magnetic study of compositions near the suppression of the  $C_2$  dome. Using a combination of neutron and X-ray scattering we observe the presence of a  $C_4$  dome in  $\text{Ca}_{1-x}\text{Na}_x\text{Fe}_2\text{As}_2$ . We compare the  $\text{Ca}_{1-x}\text{Na}_x\text{Fe}_2\text{As}_2$  phase diagram to those of  $\text{Ba}_{1-x}\text{Na}_x\text{Fe}_2\text{As}_2$  and  $\text{Sr}_{1-x}\text{Na}_x\text{Fe}_2\text{As}_2$  in order to isolate the effect of lattice anisotropy and the geometry of the  $\text{Fe}_2\text{As}_2$  layers on the formation and extent of the  $C_4$  phase and wider features of the phase diagrams in general.

## II. EXPERIMENTAL DETAILS

### A. Synthesis of $\text{Ca}_{1-x}\text{Na}_x\text{Fe}_2\text{As}_2$

Polycrystalline samples of  $\text{Ca}_{1-x}\text{Na}_x\text{Fe}_2\text{As}_2$  (with  $0.20 \leq x \leq 0.50$ ) were synthesized by sintering stoichiometric ratios of the prereacted binary precursors  $\text{CaAs}$ ,  $\text{NaAs}$ , and  $\text{Fe}_2\text{As}$  using a method similar to that reported in Reference 20. The intimately ground mixtures were

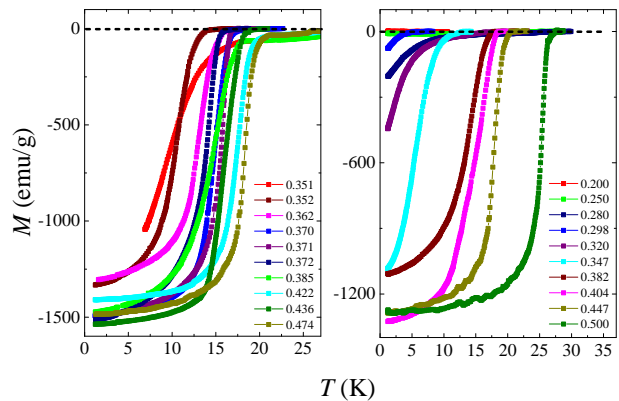


FIG. 1. The superconducting transitions for all measured powders. Magnetization normalized to mass of the samples used for neutron diffraction (at left) and X-ray diffraction (at right). All samples show either bulk superconductivity or are non-superconducting. The slight variation in diamagnetic response is consistent with small FeAs impurities seen in diffraction patterns.

loaded in alumina crucibles and arc-welded in Nb tubes under Ar atmosphere to prevent loss of the volatile alkali metal. The welded Nb tubes were sealed inside evacuated quartz tubes and sintered at 850°C for 48 hours. The resultant powder was ground with a mortar and pestle and then reannealed at 900°C. Subsequent reannealings at temperatures between 900 and 950°C with soak times between 17 - 25 hours were found necessary to ensure compositional homogeneity. Initial characterization of the dark gray powders was conducted by laboratory powder X-ray diffraction to check phase purity and crystallinity. Magnetization measurements were conducted at 0.1 Oe on a home-built SQUID magnetometer to determine the materials’ superconducting properties in addition to their compositional homogeneity through determination of  $T_c$  and the sharpness of the diamagnetic curves, (Fig. 1). Samples prepared for X-ray diffraction were typically  $\sim 1.5\text{g}$  while the samples intended for neutron diffraction were  $\sim 4.5\text{g}$ .

### B. Sample Characterization

Diffraction data were collected using the time-of-flight (TOF) neutron powder diffractometer POWGEN at the Spallation Neutron Source (SNS) of Oak Ridge National Laboratory (ORNL) and the high resolution synchrotron X-ray beamline 11BM-B of the Advanced Photon Source (APS) at Argonne National Laboratory (ANL). Data were collected between 4K and room temperature on warming. The obtained powder diffraction patterns were used with the Rietveld analysis method as implemented in the GSAS and EXPGUI software suite in order to perform detailed magnetic and nuclear structural analyses.<sup>27,28</sup> Back-to-back exponentials convoluted with

a pseudo-Voigt and microstrain broadening were used to model the TOF peak shape profile.<sup>29</sup> A pseudo-Voigt peak shape profile function 3 was used to model the data obtained from the synchrotron.

### III. RESULTS AND DISCUSSION

#### A. $C_4$ magnetic phase

Recently, we have detailed the determination of the magnetic  $C_4$  phase in a series of hole-doped ‘122’ materials  $\text{Ba}_{1-x}\text{Na}_x\text{Fe}_2\text{As}_2$ ,  $\text{Ba}_{1-x}\text{K}_x\text{Fe}_2\text{As}_2$  and  $\text{Sr}_{1-x}\text{Na}_x\text{Fe}_2\text{As}_2$ .<sup>12,20,30,31</sup> In these reports we characterized the  $C_4$  phase by an abrupt first order re-entrance at temperatures  $T < T_N$  to the tetragonal  $I4/mmm$  structure from within the well known antiferromagnetically ordered orthorhombic  $Fmmm$  structure. This structural transition is coupled to a magnetic transition where the previously in-plane Fe-site moments rotate to be co-linear to the  $c$ -axis forming a double- $\mathbf{Q}$  magnetic structure with  $P4_2/nm$  magnetic space group.<sup>31–33</sup>

Fig. 2(a) shows diffractograms of the 112 nuclear peak and the  $\frac{1}{2}\frac{1}{2}1$  and  $\frac{1}{2}\frac{1}{2}3$  magnetic peaks for  $\text{Ca}_{0.58}\text{Na}_{0.42}\text{Fe}_2\text{As}_2$  (all peaks indexed using the tetragonal symmetry of the room temperature structure). By monitoring the temperature dependence of these three peaks it is possible to distinguish between the two structural symmetries and three magnetic phases. In Fig. 2(a) the typical paramagnetic (PM)  $C_4$  to AFM  $C_2$  transition for the 42% sample is seen. At  $T = T_n = T_s \approx 105\text{K}$ , the 112 reflection splits into two distinct reflections (the 202 and 022) indicating a structural transition to the orthorhombic phase. Simultaneously, magnetic scattering can be seen at the previously background equivalent  $\frac{1}{2}\frac{1}{2}3$  and  $\frac{1}{2}\frac{1}{2}1$  positions – indicating the coupled magnetic/structural transition from the PM tetragonal phase to the AFM orthorhombic phase. The same behavior can be seen in Fig. 2(b) and (c) at  $\approx 104\text{K}$  and  $\approx 89\text{K}$  for the 40% and 45% samples respectively. The 45% sample is near the edge of the  $C_2$  dome and therefore exhibits a reduced orthorhombic distortion in the  $C_2$  phase. The orthorhombic splitting cannot be fully resolved in the x-ray diffraction data and instead manifests as a slight broadening of the 122 peak below  $T_n \approx 89\text{K}$ . At lower temperatures ( $\approx 38\text{K}$ ) the peak sharpens again indicating the return to  $C_4$  symmetry.

As the temperature is decreased below  $T_N$ , at  $T \leq 45\text{K}$  the 42% sample’s split 112 nuclear peak undergoes a sudden ( $\Delta T \sim 10\text{K}$ ) return to a single reflection. During the same temperature range, the  $\frac{1}{2}\frac{1}{2}1$  magnetic peak gains more than a factor of three in scattering intensity. Throughout  $12\text{K} < T < 45\text{K}$  the  $\frac{1}{2}\frac{1}{2}1$  peak continues to gain intensity while the  $\frac{1}{2}\frac{1}{2}3$  reflection shows little temperature dependence. This behavior is indicative of the above described spin-reorientation where the magnetic moments on the Fe sites align along the  $c$ -axis. This coupled structural/magnetic transition is characteristic

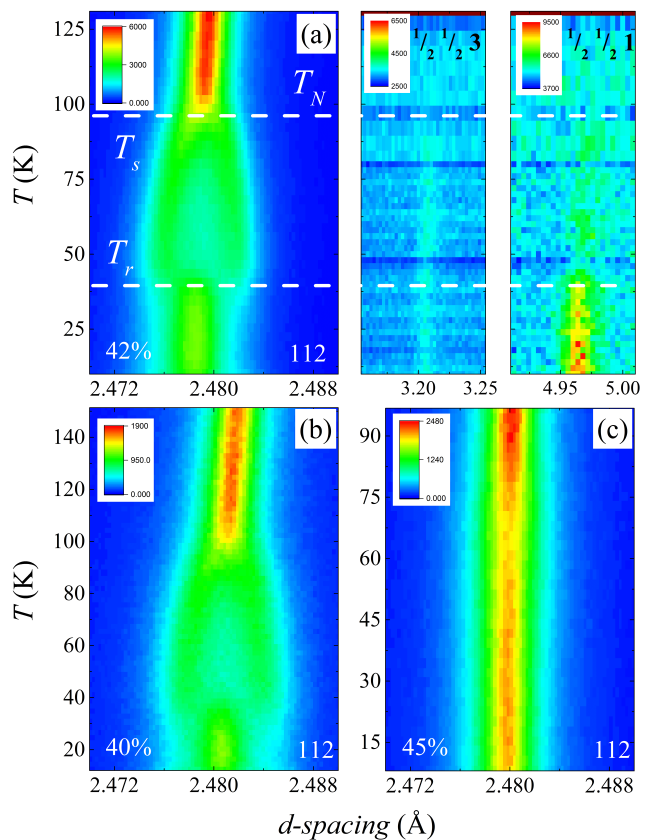


FIG. 2. Diffractograms of the 112 nuclear peak and the magnetic  $\frac{1}{2}\frac{1}{2}1$  and  $\frac{1}{2}\frac{1}{2}3$  peaks for the  $\text{Ca}_{0.58}\text{Na}_{0.42}\text{Fe}_2\text{As}_2$  sample (a). Diffractograms of the 112 peak for the  $x = 0.40$  (b) &  $0.45$  (c) samples. The diffractograms of the nuclear peak and magnetic peaks were compiled from x-ray (11BM-B) and neutron (POWGEN) diffraction patterns respectively.

of the magnetic  $C_4$  phase and is observed for all compositions of  $\text{Ca}_{1-x}\text{Na}_x\text{Fe}_2\text{As}_2$  with  $0.40 \leq x \leq 0.45$  in our samples.

Shown in Fig. 3 are neutron powder diffraction patterns collected at  $10\text{K}$  in the  $d$ -spacing range of the two magnetic reflections ( $\frac{1}{2}\frac{1}{2}1$  and  $\frac{1}{2}\frac{1}{2}3$ ). For samples with  $x \leq 0.38$  the typical  $C_2$  magnetism is observed while for the  $x = 0.42$  &  $0.44$  samples the  $C_4$  structure appears — clear from the increased relative intensity of the  $\frac{1}{2}\frac{1}{2}1$  peak compared to lower compositions despite the expected suppression of the magnetic moment with increased doping. Interestingly, for the 47% sample the  $C_2$  magnetism returns indicating that the  $C_4$  dome is buttressed at both higher and lower concentrations by the standard AFM stripe magnetism. While not observed in  $\text{Ba}_{1-x}\text{Na}_x\text{Fe}_2\text{As}_2$  we recently reported a similar behavior in  $\text{Sr}_{1-x}\text{Na}_x\text{Fe}_2\text{As}_2$  and  $\text{Ba}_{1-x}\text{K}_x\text{Fe}_2\text{As}_2$ .<sup>12,14,20,31</sup> The significance of this re-entrance in composition space will be discussed in Section III C.

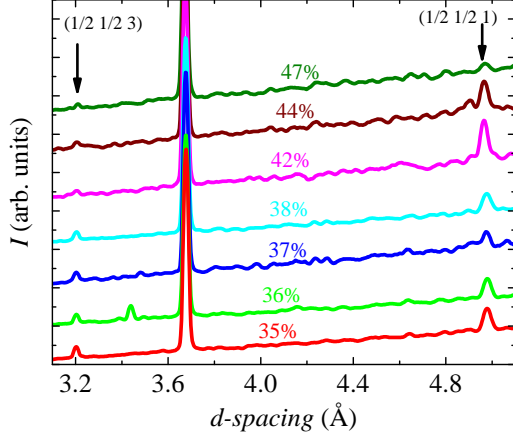


FIG. 3. Neutron diffraction patterns collected on POWGEN at 10K for a series of compositions near the  $C_4$  dome. Indicated with arrows are the  $\frac{1}{2} \frac{1}{2} 3$  and  $\frac{1}{2} \frac{1}{2} 1$  magnetic reflections. Patterns are arbitrarily offset to aid in visual comparison.

### B. Re-entrance of AFM $C_2$

A notable feature of the diffractograms shown in Fig. 2 is the apparent broadness of the 112 peak at low temperatures as compared to the peak in the PM tetragonal phase. Previously, we reported a similar behavior in  $\text{Ba}_{1-x}\text{Na}_x\text{Fe}_2\text{As}_2$  which was attributed to a finite percentage of the sample remaining in the orthorhombic phase.<sup>12</sup> However, as will be shown, here the broadness is caused in part by a more complicated phase diagram in the  $\text{Ca}_{1-x}\text{Na}_x\text{Fe}_2\text{As}_2$  material.

Fig. 4 (a) shows the refined  $a$  and  $b$  lattice parameters for a series of compositions near the  $C_4$  dome. For the 40% sample, the presence of both tetragonal and orthorhombic lattice parameters below  $T_r$  results from a mixed phase refinement. As shown in Fig. 4(c-d) the orthorhombic 202 and 022 (200 and 020) peaks are always present even to base temperature. Therefore, as in  $\text{Ba}_{1-x}\text{Na}_x\text{Fe}_2\text{As}_2$ , for  $T < T_r$   $\text{Ca}_{0.60}\text{Na}_{0.40}\text{Fe}_2\text{As}_2$  has domains of both  $C_4$  and  $C_2$  symmetries.

However, the intensity of the orthorhombic peaks does not monotonically decrease or remain constant as should be expected for the case of mixed phases due to either chemical inhomogeneity or intrinsic phase separation. Instead, for  $T < 20\text{K}$  the intensities of the orthorhombic peaks are seen to increase while the central tetragonal peak decreases (Fig. 4 (c-d)). Extracting the weighted phase fraction from mixed phase refinements of the 40% sample (Fig. 4(b)) the sample is seen to begin returning to the orthorhombic symmetry from within the  $C_4$  phase. Between 21K (the maximum phase fraction of  $C_4$ ) and 12K (lowest measured temperature) the phase fraction of the  $C_2$  phase changes from 37% to 62% meanwhile the  $C_4$  phase drops from being the majority phase at 63% to the minority phase at 38%. Similar behavior is also

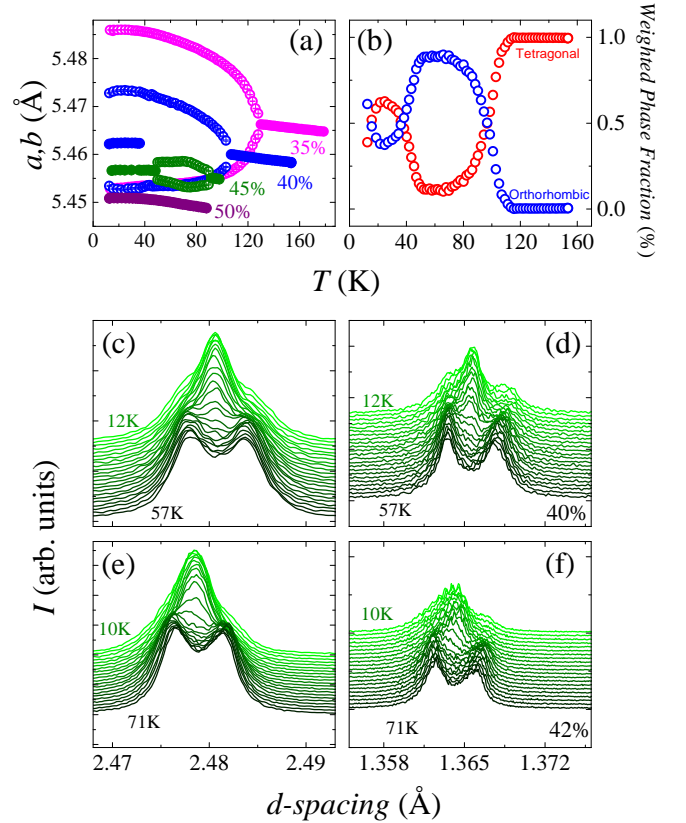


FIG. 4.  $a$  and  $b$  lattice parameters of the  $x = 0.35, 0.40, 0.45$ , &  $0.50$  samples extracted from Rietveld refinements. The  $a$  lattice parameter for the tetragonal phases is indicated by filled symbols and has been scaled by a factor of  $\sqrt{2}$  to aid in visual comparison (a). The refined phase fraction of the tetragonal (red) and orthorhombic (blue) phases in a mixed phase refinement for the 40% sample (b). Waterfall plots showing the temperature dependence of the 112 (c & e) and 220 (d & f) nuclear peaks of the 40% and 42% samples respectively.

seen in the 42% sample (Fig. 4 (e-f)) however, less of the sample exhibits this phase re-entrance and so it is not possible to perform reliable and stable mixed phase refinements. Nonetheless, qualitatively the behavior of these two compositions is similar with a re-entrance of part of the sample to the  $C_2$  symmetry from within the  $C_4$  phase.

It is important to note that this is a true second re-entrance to the  $C_2$  structure and not an artifact born of chemical inhomogeneity; the commensurate shift in opposite directions of the two phases' weighted fractions indicates that the  $C_4$  phase is undergoing another phase transition (characterized as  $T_{r2}$ ) back to the  $C_2$  symmetry. Interestingly,  $T_{r2}$  occurs simultaneous to the superconducting transition  $T_c$ , within the resolution of our measurements for the 40% sample. A similar combined magnetic, structural and superconducting transition for  $\text{Ba}_{0.74}\text{K}_{0.26}\text{Fe}_2\text{As}_2$  has been reported and this behavior indicates the strong competition between superconduc-

tivity and the magnetic  $C_4$  phase.<sup>14,31</sup>

While, such a  $C_2$  re-entrance has been reported in  $\text{Ba}_{1-x}\text{K}_x\text{Fe}_2\text{As}_2$  (Reference 31) and its significance discussed (Reference 14), it has not been seen in any other 122 system as far as the authors of this paper are aware. It is not obvious why  $\text{Ca}_{1-x}\text{Na}_x\text{Fe}_2\text{As}_2$  and  $\text{Ba}_{1-x}\text{K}_x\text{Fe}_2\text{As}_2$  should show  $C_2$  re-entrance while  $\text{Ba}_{1-x}\text{Na}_x\text{Fe}_2\text{As}_2$  and  $\text{Sr}_{1-x}\text{Na}_x\text{Fe}_2\text{As}_2$  do not. Though  $\text{Ba}_{1-x}\text{K}_x\text{Fe}_2\text{As}_2$  is notable for the brevity in composition and temperature space of the  $C_4$  phase — indicating its relative instability to the  $C_2$  phase — in  $\text{Ca}_{1-x}\text{Na}_x\text{Fe}_2\text{As}_2$  the  $C_4$  phase has a relatively robust extent in phase space. The compositional range of  $C_4$  in  $\text{Ca}_{1-x}\text{Na}_x\text{Fe}_2\text{As}_2$  ( $\Delta x \sim 0.05$ ) is comparable to that found in  $\text{Ba}_{1-x}\text{Na}_x\text{Fe}_2\text{As}_2$ . Yet, to date no such re-entrance is found for  $\text{Ba}_{1-x}\text{Na}_x\text{Fe}_2\text{As}_2$  despite several careful studies.<sup>12,34</sup> Therefore, this re-entrant  $C_2$  is likely born of more subtle effects and warrants further study.

Interestingly, careful inspection of the lattice parameters and peak positions at the  $C_4$  transition in the mixed phase compositions reveal remarkably little change in the lattice parameters between the standard  $C_2$  phase and the coexistent  $C_2$  phase (Fig. 4). Should the mixed phase states be due to a chemical homogeneity then it should be expected that the remnant portion of the sample in the  $C_2$  phase would exhibit a greater orthorhombic distortion ostensibly being of lower Na concentration. However, as seen in Fig. 4(a) the  $a$  and  $b$  lattice parameters of the  $C_2$  phase across the  $C_4$  transition are nearly constant indicating the possibility that it is not some compositionally distinct portion of the sample which is remaining  $C_2$  but that some other effect must be influencing the phase behavior.

In Ref. 31 we reported a similar behavior in the  $\text{Ba}_{1-x}\text{K}_x\text{Fe}_2\text{As}_2$  compound and attributed the extra influence as due to possible localized defects in parts of the sample. Since then, theory has shown that impurity scattering can play a significant role in the stabilization of the  $C_4$  phase.<sup>17</sup> In their work, Hoyer *et al.* show that intra-band electron scattering due to crystallographic defects stabilize the  $C_4$  phase at lower doping concentrations - at the beginning of the  $C_4$  dome. However, no such effect is found on the higher doped side of the dome in agreement with our observation of mixed phase samples at the onset of  $C_4$  in composition but not at higher concentrations. While, admittedly, it is difficult to decouple such defects from chemical inhomogeneity (e.g. inhomogeneity in the distribution of the dopant atom) our data indicate that there is another variable other than composition which also affects the phase behavior of the material. Further experimental work is needed to determine the exact role defects play in stabilizing the  $C_4$  either through irradiation (as suggested in Reference 17), through co-substitution with an isovalent atom or through mechanically introduced crystallographic defects.

TABLE I. Fitted composition and structural and magnetic transition temperatures. Fit compositions were determined through the use of a Vegard's Law like behavior of the  $a$  lattice parameter (see Reference 20 for a description of the procedure used for sample composition determination). Critical temperatures ( $T_c$ ,  $T_s$ ,  $T_N$ ,  $T_r$  and  $T_{r2}$ ) were determined using a consistently applied methodology (see text for details).

$x_{fit}$	$T_c$	$T_N$	$T_s$	$T_r$	$T_{r2}$
neutron					
0.35(2)	11(1)	119(3)	119(5)		
0.35(2)	12(1)				
0.36(2)	14(1)				
0.37(2)	16(1)	113(5)	115(5)		
0.37(2)	16(1)	110(4)	112(5)		
0.38(2)	16(1)	108(4)	106(5)		
0.42(2)	18(1)	105(4)		40(4)	12(4)
0.44(2)	17(1)	101(4)		52(4)	
0.47(2)	19(1)				
X-ray					
0.20(2)					
0.25(2)					
0.30(2)	3(1)				
0.32(2)	5(1)				
0.35(2)	10(2)		126(4)		
0.38(2)	17(1)		109(4)		
0.40(2)	18(2)		104(4)	24(4)	18(2)
0.42(2)	18(1)		105(4)	40(5)	
0.45(2)	19(1)		89(4)	38(5)	
0.50(2)	26(1)				

### C. Phase Diagram

Table I lists the transition temperatures of all measured samples. In order to consistently determine the critical temperatures across all samples (considering many have competing order parameters) the typical power-law fitting method used to determine  $T_N$  and  $T_s$  was eschewed.<sup>30,35–37</sup> Instead, the methodology described in Reference 20 was employed. Critical temperatures were determined by comparing linear fits of the order parameter immediately before and after the transition. The order parameters used were: magnetization ( $M$ ), magnetic moment ( $m$ ) and orthorhombic distortion ( $\delta = (a-b)/(a+b)$ ). While the former two were used for  $T_c$  and  $T_N$  respectively the latter was used for  $T_s$  as well as  $T_{r2}$ . For  $T_r$ , the collapse of  $\delta$  was used. In this manner modifications to the expected power-law behavior due to the presence of a third (and fourth) phase transition, specifically in samples exhibiting  $T_r$ 's, could be mitigated and a consistent method used across all transitions and samples.

Fig. 5 shows the graphical representation of Table I forming a phase diagram for  $\text{Ca}_{1-x}\text{Na}_x\text{Fe}_2\text{As}_2$ . While sharing general features with the previously reported  $\text{Ca}_{1-x}\text{Na}_x\text{Fe}_2\text{As}_2$  phase diagrams (References 22 and 21), our use of fine steps in composition, specifically towards the edge of the  $C_2$  dome, reveals a previously unreported  $C_4$  dome in this hole-doped  $\text{CaFe}_2\text{As}_2$  system. The  $C_4$



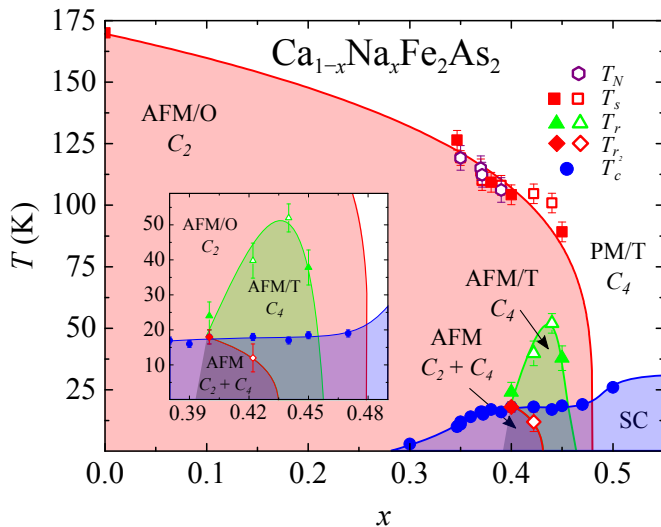


FIG. 5. Phase diagram of  $\text{Ca}_{1-x}\text{Na}_x\text{Fe}_2\text{As}_2$ . Filled and open symbols are transitions determined from X-ray and neutron data, respectively. The parent compound's transition temperature was taken from Reference 38. The red, blue and green shaded areas represent the AFM orthorhombic, superconducting and AFM tetragonal phases respectively. The shaded region indicates phase coexistence between the  $C_4$  phase and a re-entrant  $C_2$  phase. Coincident structural and magnetic transitions are represented for each phase by a solid line. Inset: an enlarged view showing details of the  $C_4$  dome.

phase first appears at  $x \sim 0.40$  at  $T = 24\text{K}$  and continues in composition space until  $x \sim 0.47$  where the AFM  $C_2$  phase returns describing a  $C_4$  dome with  $\Delta x = 0.05$  in composition. The compositional dependence of  $T_r$  in this range is roughly parabolic with a maximum  $T_r$  of 52K at  $x = 0.44$  which then decreases with further doping. Between  $0.47 < x < 0.50$  magnetism and the accompanying structural distortion are completely suppressed describing the closing of the  $C_2$  dome.

As previously reported, superconductivity is first seen at  $x = 0.30$  where it monotonically rises with composition until reaching 26K for the 50% sample - the highest composition measured in this study. Interestingly, at the onset in composition of the  $C_4$  phase  $T_c$  is seen to plateau exhibiting no composition dependence (within the resolution of our measurements) over  $0.40 \leq x \leq 0.45$ . This suppression of  $T_c$  by  $C_4$  indicates the strong competition between the  $C_4$  phase magnetic ordering and superconductivity as recently suggested in a first principle calculations report of the  $C_4$  phase.<sup>15</sup>

The previously discussed re-entrant  $C_2$  phase is visible in Fig. 5 as a shaded region. Qualitatively, the behavior of this mixed phase region is very similar to that observed previously in Ref. 14 and 31 and explained theoretically in Ref. 15 for the  $\text{Ba}_{1-x}\text{K}_x\text{Fe}_2\text{As}_2$  material. It is noteworthy that all three systems show a decreasing  $T_{r_2}$  with increasing composition resulting in the re-entrance only affecting the lower doped side of the  $C_4$  dome. Furthermore, we find that  $T_{r_2} \leq T_c$  — consistent with recent re-

ports which have suggested the  $C_4$  phase's doubly gapped Fermi surface competes more strongly with superconductivity than the singly gapped  $C_2$  phase.<sup>15,16</sup>

## D. Comparison of Hole-doped 122's

### 1. Phase Diagrams and Extent of the $C_4$ phase

Fig. 6 (a) plots the phase diagrams of  $\text{Ba}_{1-x}\text{Na}_x\text{Fe}_2\text{As}_2$ ,  $\text{Sr}_{1-x}\text{Na}_x\text{Fe}_2\text{As}_2$  and  $\text{Ca}_{1-x}\text{Na}_x\text{Fe}_2\text{As}_2$  on shared axes (the former two compounds phase diagrams are generated from data we reported in Refs. 12 and 20 respectively). As noted in Ref. 39, the  $T_N$  of the parent compounds is non-monotonic going up the alkali-earth metal group from Ba to Sr to Ca with  $T_N$  of 140, 210 and 170K, respectively.<sup>30,38,40</sup> Setting aside the composition dependence, it is somewhat unsurprising that the maximum  $T_r$  for each system appears to scale with  $T_N$  going from 45K to 65K to 52K for Ba, Sr and Ca.<sup>20,30,41</sup>

Naively, the scaling of the  $T_N$  of the parent compound with  $T_r$  seems reasonable assuming a higher magnetic ordering temperature would require a larger amount of charge doping to disrupt. This would then extend the  $C_2$  dome out to higher compositions and consequently allow for a more fully formed  $C_4$  dome. However, several features of this comparison dispute this explanation. Unexpectedly, though  $T_N$  of the parent decreases between Sr and Ca the extent of the  $C_2$  dome is nearly the same (with a shared critical composition of  $x \sim 47\%$ ). Furthermore, despite this and the higher  $T_N$  of  $\text{SrFe}_2\text{As}_2$ ,  $\text{Ca}_{1-x}\text{Na}_x\text{Fe}_2\text{As}_2$  does not exhibit  $C_4$  re-entrant behavior until significantly higher dopant concentrations ( $x \sim 0.29$  for  $\text{Sr}_{1-x}\text{Na}_x\text{Fe}_2\text{As}_2$  compared to  $x \sim 0.40$  for  $\text{Ca}_{1-x}\text{Na}_x\text{Fe}_2\text{As}_2$ ) indicating a more complex relationship between the parent compound's  $T_N$  and the effect of  $\text{Na}^+$  doping.

As discussed in Ref. 39 the non-monotonic behavior of the  $T_N$  between the three parent compounds as well as the itinerant electronic behavior indicates that the changes in the magnetic and electronic behavior must be due to structural changes in the material. Such considerations can be extended to these three charge doped systems due to the direct correspondence at any given dopant concentration to a similar charge doping in all systems. The significant difference between the three systems for a given  $\text{Na}^+$  concentration is the average size of the A-site ion which will impact the overall structure of the unit cell as well as the important internal bonding parameters and affect the differences seen in Fig. 6(b-d). These effects will be the focus of Section III D 3.

### 2. Structure and Magnetism

The observation of the  $C_4$  phase in  $\text{Ca}_{1-x}\text{Na}_x\text{Fe}_2\text{As}_2$  makes it the fourth member of the hole-doped '122' family to exhibit this phase, demonstrating that

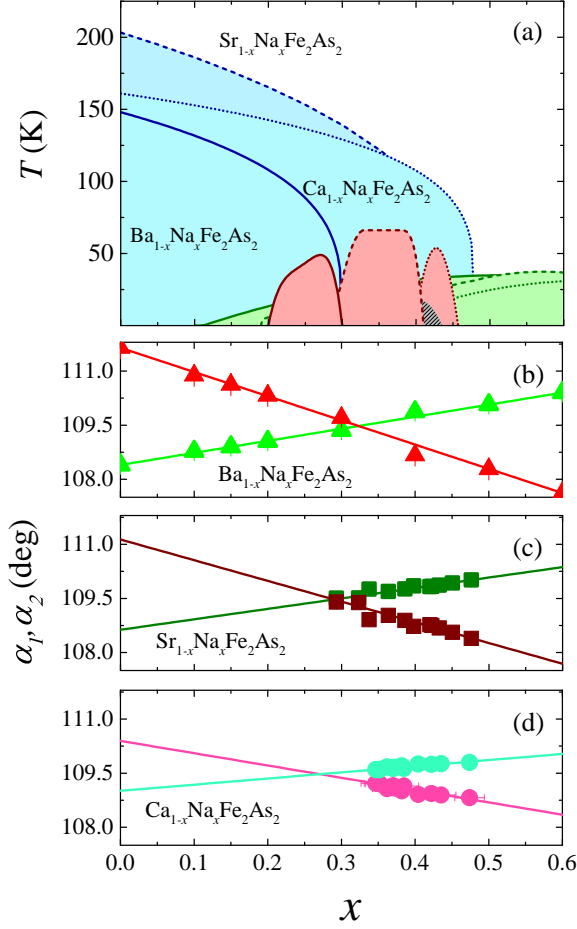


FIG. 6. Phase diagrams of the three  $\text{Na}^+$  doped 122 systems overlaid (a). The solid, dashed and short dashed lines correspond to the  $\text{Ba}_{1-x}\text{Na}_x\text{Fe}_2\text{As}_2$ ,  $\text{Sr}_{1-x}\text{Na}_x\text{Fe}_2\text{As}_2$  and  $\text{Ca}_{1-x}\text{Na}_x\text{Fe}_2\text{As}_2$  phase boundaries respectively. While the blue, red and green shaded regions correspond to the AFM  $C_2$ , AFM  $C_4$  and SC phases respectively. The composition dependence of the FeAs layer tetrahedral angles at 10K for  $\text{Ba}_{1-x}\text{Na}_x\text{Fe}_2\text{As}_2$  (b),  $\text{Sr}_{1-x}\text{Na}_x\text{Fe}_2\text{As}_2$  (c) and  $\text{Ca}_{1-x}\text{Na}_x\text{Fe}_2\text{As}_2$  (d). Values for the angles of  $\text{Ba}_{1-x}\text{Na}_x\text{Fe}_2\text{As}_2$  and  $\text{Sr}_{1-x}\text{Na}_x\text{Fe}_2\text{As}_2$  were taken from Refs. 30 and 20 respectively.

it is an intrinsic (rather than coincidental) feature of these materials. Considering the three  $\text{Na}^+$  doped compounds ( $\text{Ba}_{1-x}\text{Na}_x\text{Fe}_2\text{As}_2$ ,  $\text{Sr}_{1-x}\text{Na}_x\text{Fe}_2\text{As}_2$  and  $\text{Ca}_{1-x}\text{Na}_x\text{Fe}_2\text{As}_2$ ) allows for the influence of structural changes on the formation of the  $C_4$  phase to be isolated from the effects of charge doping.

The ionic radius of the  $A$ -site in  $A\text{Fe}_2\text{As}_2$  decreases from  $1.42\text{\AA}$  to  $1.26\text{\AA}$  to  $1.12\text{\AA}$  as the  $A$ -site ion goes up the alkaline earth metals from Ba to Sr to Ca respectively.<sup>42</sup> This decrease should be expected to cause a contraction of the unit cell volume which in turn will tune the magnetic properties by changing the Fe-Fe distances as well as the  $\text{Fe}_2\text{As}_2$  interlayer spacings. Fig. 7(a) shows the unit cell volume ( $V$ ) of the three  $\text{Na}^+$  doped

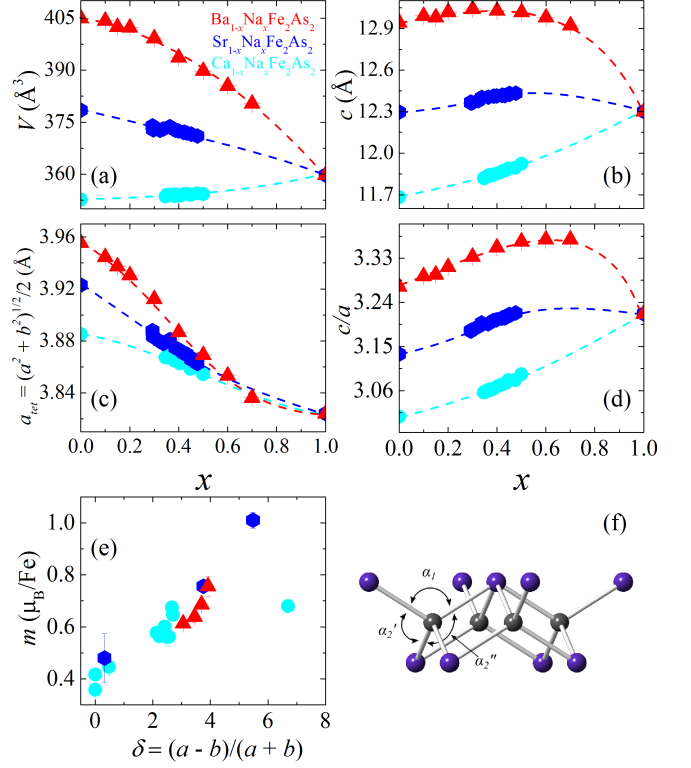


FIG. 7. Compositional dependence of the unit cell: volume (a),  $c$  axis (b),  $a_{tet}$  direction (c) and  $c/a$  ratio (d) for the three  $\text{Na}^+$  doped 122 systems at 300K. The refined magnetic moment plotted as a function of the orthorhombic order parameter  $\delta$  (where  $\delta$  has been scaled by a factor of  $10^3$ ) for data collected at 10K (e). The  $\text{Fe}_2\text{As}_2$  layer with the  $\alpha_1$  and two  $\alpha_2$  angles indicated (f). Data for  $\text{Ba}_{1-x}\text{Na}_x\text{Fe}_2\text{As}_2$  and  $\text{Sr}_{1-x}\text{Na}_x\text{Fe}_2\text{As}_2$  were taken from Ref. 30 and 20 respectively.

compounds. As expected,  $V$  decreases from  $\text{BaFe}_2\text{As}_2$  to  $\text{SrFe}_2\text{As}_2$  to  $\text{CaFe}_2\text{As}_2$  in nearly equal steps of approximately -6.5% and -7.0% respectively.

However, this contraction is anisotropic. Fig. 7(b) and (c) show the  $a_{tet}$  and  $c$  lattice parameters. While, both contract as the  $A$ -site ion is moved up the group, the  $c$ -axis is significantly more sensitive changing by -5% for each step up compared to approximately -1% for the  $a_{tet}$  direction. This is quantitatively measured with the anisotropy ratio  $c/a$  (Fig. 7(d)) which steadily decreases from Ba to Ca. This anisotropic contraction of the unit cell should be expected to significantly affect the geometry of the  $\text{Fe}_2\text{As}_2$  layers and the Fe-Fe spacing both in and out of plane as will be discussed in Section III D 3.

The strong magneto-elastic coupling in the ‘122’ materials is well characterized at this point both experimentally and theoretically.<sup>5,10,11,43–45</sup> In Fig. 7 (e) the magnetic order parameter ( $m$ ) is plotted as a function of the structural order parameter ( $\delta$ ) for all three systems at base temperature. Remarkably, despite the differences in the compounds’  $C_2$  phase composition dependence and absent any scaling, the three systems appear to fall on



the same  $m(\delta)$  curve. As expected  $m(\delta)$  increases monotonically between  $0 \leq \delta \leq 5.5$  (where  $m(0)$  accounts for AFM  $C_4$  samples) indicating the relationship between the magnitude of the structural distortion and the strength of the magnetic ordering.

Whether the two order parameters are related linearly or quadratically has long been debated.<sup>37</sup> While Fig. 7 seems to indicate a quadratic relationship for  $\delta < 5.5$  the quality of the data does not afford much certainty. However, it is interesting to note the similarity between the three systems. In a linear approximation (as suggested in Ref. 46 and derived explicitly in Ref. 43)  $\delta(m)$  has the form  $\delta = \alpha m$  where  $\alpha$  is a constant related to the strength of the magnetoelastic coupling, the shear modulus and the chemical doping. That all three systems fall on the same curve indicates the similarity between these important parameters despite the different parent compounds.

For  $\delta > 5.5$ ,  $m$  decreases with increasing  $\delta$ . This region corresponds to the under-doped  $\text{Ca}_{1-x}\text{Na}_x\text{Fe}_2\text{As}_2$  samples and is similar to the unexpected decrease in  $m$  seen in the parent compounds between  $\text{SrFe}_2\text{As}_2$  and  $\text{CaFe}_2\text{As}_2$ . This is likely related to the nonmonotonic behavior of  $T_N$  and  $m$  as a function of unit cell volume for  $\text{Ba}_{1-x}\text{Sr}_x\text{Fe}_2\text{As}_2$  and  $\text{Sr}_{1-x}\text{Ca}_x\text{Fe}_2\text{As}_2$  reported in Ref. 39. Unfortunately, due to the focus of the present study on compositions towards the edge of the  $C_2$  dome we do not have data on significantly underdoped compositions leaving a large gap between the maximum  $m_{\max}(\delta)$  and  $\delta_{\max}$  limiting our ability to fit the curve in this region.

### 3. Internal Parameters

As shown in Fig. 7(d) there is a significant decrease in the lattice anisotropy among the three parent compounds which persists even to our highest measured Na concentrations. It should be expected then that the  $\text{Fe}_2\text{As}_2$  layers (which are characterized by: the Fe-Fe and Fe-As bond lengths as well as the As-Fe-As angles (Fig. 7(f)) have significantly different geometries in these three materials.

Recently, we suggested the importance of the  $\text{Fe}_2\text{As}_2$  layers' bonding parameters to the stabilization of the  $C_4$  phase.<sup>20</sup> In  $\text{Sr}_{1-x}\text{Na}_x\text{Fe}_2\text{As}_2$  the  $C_4$  phase was found to occur in a small range of As-Fe-As bond angles where the  $\text{FeAs}_4$  approached perfect tetrahedra. We suggested that the return locally to a higher symmetry in the  $\text{Fe}_2\text{As}_2$  layers might create an electronic instability which contributes to the recovery of magnetic degeneracy and a consequent return to  $C_4$  symmetry. It is then informative to look at all three Na doped systems and quantify how these bond angles change with structure and how this relates to the observed phase diagrams.

Fig. 8 shows the Fe-As and A-As bond lengths for the three Na doped materials. As reported for  $\text{Sr}_{1-x}\text{Na}_x\text{Fe}_2\text{As}_2$  the Fe-As bond length is nearly constant across all measured Na concentrations and even, strik-

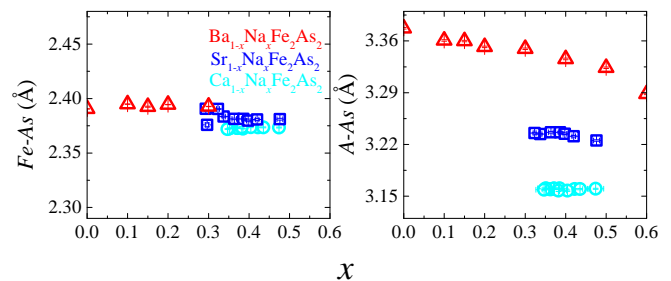


FIG. 8. Fe-As (left) and A-Fe(right) bond lengths of the three Na doped 122 materials at 10K.

ingly, across the different materials. However, as shown in Fig. 7(a) and (b) there is a significant reduction of the unit cell volume and of the  $c$ -axis across the three materials which must result in changes to the internal bonding parameters. Interestingly, this contraction does not affect the robust Fe-As bond, but is instead compensated for in the A-site to As bond length (Fig. 8) which contracts significantly between the three systems following the trend seen in  $V$  and the  $c$  axis.

The Fe-Fe bond length is proportional to the  $a$  lattice parameter due to the Fe atom's location on a special crystallographic site. Therefore, the previously discussed  $\sim 1\%$  contraction of the  $a$  axis between parent compounds corresponds to an identical contraction of the Fe-Fe distance in response to the smaller A site ion. On the other hand, the effects of  $\text{Na}^+$  doping on the Fe-Fe bond has been discussed previously in Ref. 30, and results in the reduction of antibonding between neighboring Fe and therefore a contraction of Fe-Fe bond distance. As the A-site is changed between the systems from Ba to Ca the Fe-Fe bond length contracts. Furthermore, as Na is doped into each parent compound the Fe-Fe bond-length also contracts. The combination of these two effects leads to the decreases in  $a$  seen in Fig. 7(c) and the latter effect causes the severely reduced  $a$  seen in the end compound  $\text{NaFe}_2\text{As}_2$ .

The sum of these effects indicates that the decreasing  $c/a$  ratio from  $\text{BaFe}_2\text{As}_2$  to  $\text{SrFe}_2\text{As}_2$  to  $\text{CaFe}_2\text{As}_2$  has different manifestations along the different crystallographic directions for the  $\text{Fe}_2\text{As}_2$  layers. The large contraction along  $c$  is a result of A-As bond lengths leaving the FeAs bond unchanged while the contraction along  $a$  directly corresponds to a reduction in spacing between Fe atoms in the  $\text{Fe}_2\text{As}_2$  layer's square planar Fe sublattice. As seen in the lower panels of Fig. 6 the result is a change in the As-Fe-As angles  $\alpha_1$  and  $\alpha_2$ .  $\text{BaFe}_2\text{As}_2$  which has the largest  $c/a$  ratio also has the largest splitting between the two angles  $\Delta\alpha = |\alpha_1 - \alpha_2| = 3.20^\circ$ .  $\Delta\alpha$  decreases in  $\text{SrFe}_2\text{As}_2$  and  $\text{CaFe}_2\text{As}_2$  to  $2.58^\circ$  and  $1.43^\circ$  respectively.

As  $\text{Na}^+$  is doped into these materials the two As-Fe-As angles begin to converge. The Fe-Fe contraction and Fe-As rigidity drive the wider  $\alpha_1$  angle to close and the smaller  $\alpha_2$  angle to open until the two angles cross at the perfect tetrahedral angle ( $109.46^\circ$ ) at  $x = 0.32$ ,

0.29 and 0.27, for  $\text{Ba}_{1-x}\text{Na}_x\text{Fe}_2\text{As}_2$ ,  $\text{Sr}_{1-x}\text{Na}_x\text{Fe}_2\text{As}_2$  and  $\text{Ca}_{1-x}\text{Na}_x\text{Fe}_2\text{As}_2$  respectively. Upon further doping the angles separate with  $\alpha_1 < \alpha_2$ .

At various times the role of  $\alpha_1$  and  $\alpha_2$  as important parameters in determining the electronic structure of these materials has been explored.<sup>47–51</sup> The bond angles are closely related to the pnictogen height and determine the overlap between the pnictogen's  $p$  orbitals and the Fe-sites'  $3d$  orbitals. In Ref. 49 first principles calculations predict that the Fermi-surface becomes more degenerate as  $\Delta\alpha \rightarrow 0$ . It is possible that the recipe for  $C_4$  involves balancing this return to a higher symmetry FS with the needed isotropy between the size of the hole and electron FS sheets known to be necessary to stabilize  $C_4$ .<sup>12</sup> Such a description would explain why  $C_4$  is seen only over a short range of compositions where these two conditions are met within the  $C_2$  dome. However, most reports using first principle calculations to study the importance of the  $\text{Fe}_2\text{As}_2$  layer geometry were performed before the discovery of the  $C_4$  phase. It would be useful now to revisit these discussions in light of this new phase.

#### IV. CONCLUSIONS

We report the observation of the magnetic  $C_4$  phase in a fourth member of the hole-doped 122 family of FBS —  $\text{Ca}_{1-x}\text{Na}_x\text{Fe}_2\text{As}_2$  — as determined by high resolution neutron and X-ray diffraction experiments. A  $C_4$  dome is seen for compositions  $0.40 \leq x \leq 0.45$  with a maximum  $T_r$  of  $\sim 52\text{K}$ . For higher compositions  $0.45 < x \leq 0.47$  only  $C_2$  magnetism is observed describing a  $C_4$  dome which closes before the complete suppression of magnetic ordering. On the low composition side of the  $C_4$  phase a re-entrance to the  $C_2$  phase is observed which coincides with the arrival of superconductivity in the  $x = 0.40$  sample.

Compared to the previous  $C_4$  containing 122's we report a phase diagram which has a mix of the previously discrete features, such as the separated  $C_2$  and  $C_4$  domes seen only in  $\text{Sr}_{1-x}\text{Na}_x\text{Fe}_2\text{As}_2$  and the re-entrant

$C_2$  only detected in  $\text{Ba}_{1-x}\text{K}_x\text{Fe}_2\text{As}_2$ . These observations seem to indicate important subtle structural effects as the controlling factors for the formation of the  $C_4$  phase which are considered in a comparison of the three  $\text{Na}^+$  doped materials —  $\text{Ba}_{1-x}\text{Na}_x\text{Fe}_2\text{As}_2$ ,  $\text{Sr}_{1-x}\text{Na}_x\text{Fe}_2\text{As}_2$  and  $\text{Ca}_{1-x}\text{Na}_x\text{Fe}_2\text{As}_2$ .

An anisotropic contraction of the unit cell is observed upon changing the  $A$  site from Ba to Sr to Ca caused by a markedly larger sensitivity of the  $c$  axis to the  $A$  site ion than the  $a$  axis. By comparing the internal parameters it is found that the Fe-Fe and Fe-As bond lengths are robust to changes in the  $A$  site with the consequent lattice response resulting from  $A$ -Fe bond lengths and As-Fe-As bond angles. An intriguing correlation between the As-Fe-As bond angle and the  $C_4$  phase is reported where for all three  $\text{Na}^+$  doped materials the  $C_4$  phase occurs in close proximity to the perfect tetrahedral angle. We suggest the possibility of this local return to higher symmetry as a factor in the  $C_2/C_4$  structure instability and advocate for a revisit of the first principle studies of the  $\text{Fe}_2\text{As}_2$  layer geometry's effect on the 122's phase stability.

#### ACKNOWLEDGMENTS

The work at the Materials Science Division of Argonne National Laboratory was supported by the US Department of Energy, Office of Science, Materials Sciences and Engineering Division. Research conducted at ORNL's High Flux Isotope Reactor and Spallation Neutron Source was sponsored by the Scientific User Facilities Division, Office of Basic Energy Sciences, US Department of Energy. Use of the Advanced Photon Source at Argonne National Laboratory was supported by the U.S. Department of Energy, Office of Science, Office of Basic Energy Sciences under Contract No. DE-AC02-06CH11357. The authors thank A. Huq and P. Whitfield for providing help during experimental data collection and analysis.

---

\* corresponding author taddeikm@ornl.gov

<sup>1</sup> Y. Kamihara, H. Hiramatsu, M. Hirano, R. Kawamura, H. Yanagi, T. Kamiya, and H. Hosono, *Journal of the American Chemical Society* **128**, 10012 (2006).

<sup>2</sup> D. N. Basov and V. Chubukov, *Nature Physics* **7** (2011), doi:10.1038/nphys1975.

<sup>3</sup> M. Rotter, M. Tegel, D. Johrendt, I. Schellenberg, W. Hermes, and R. Pöttgen, *Physical Review B* **78**, 020503 (2008).

<sup>4</sup> A. D. Christianson, E. A. Goremychkin, R. Osborn, S. Rosenkranz, M. D. Lumsden, C. D. Malliakas, I. S. Todorov, H. Claus, D. Y. Chung, M. G. Kanatzidis, R. I. Bewley, and T. Guidi, *Nature Letters* **456**, 930 (2008).

<sup>5</sup> S. Avci, O. Chmaissem, E. A. Goremychkin,

S. Rosenkranz, J. P. Castellán, D. Y. Chung, I. S. Todorov, J. A. Schlueter, H. Claus, M. G. Kanatzidis, A. Daoud-Aladine, D. Khalyavin, and R. Osborn, *Physical Review B* **83** (2011), 10.1103/PhysRevB.83.172503.

<sup>6</sup> H. H. Kuo, M. C. Shapiro, S. C. Riggs, and I. R. Fisher, *Physical Review B* **88**, 085113 (2013).

<sup>7</sup> J. H. Chu, H. H. Kuo, J. G. Analytis, and I. R. Fisher, *Science* **337**, 710 (2012).

<sup>8</sup> S. Kasahara, H. J. Shi, K. Hashimoto, S. Tonegawa, Y. Mizukami, T. Shibauchi, K. Sugimoto, T. Fukuda, T. Terashima, A. H. Nevidomskyy, and Y. Matsuda, *Nature* **486**, 382 (2012).

<sup>9</sup> M. Yi, D. Lu, J.-H. Chu, J. Analytis, A. Sorini, A. Kemper, B. Moritz, S.-K. Mo, R. Moore, M. Hashimoto, W. Lee,

- Z. Hussain, T. Devereaux, I. Fisher, and Z.-X. Shen, Proceedings of the National Academy of Sciences **108**, 6878 (2011).
- <sup>10</sup> C. Dhital, Z. Yamani, W. Tian, J. Zeretsky, A. S. Sefat, Z. Wang, R. J. Birgeneau, and S. D. Wilson, Physical Review Letters **108**, 087001 (2012).
  - <sup>11</sup> R. M. Fernandes, A. E. Böhmer, C. Meingast, and J. Schmalian, Physical Review Letters **111**, 137001 (2013).
  - <sup>12</sup> S. Avci, O. Chmaissem, J. M. Allred, S. Rosenkranz, I. Eremin, A. V. Chubukov, D. E. Bugaris, D. Y. Chung, M. G. Kanatzidis, J. P. Castellan, J. A. Schlueter, H. Claus, D. D. Khalyavin, P. Manuel, A. Daoud-Aladine, and R. Osborn, Nature Communications **5** (2014), 10.1038/ncomms4845.
  - <sup>13</sup> J. M. Allred, K. M. Taddei, D. E. Bugaris, M. J. Krogstad, S. H. Lapidus, D. Y. Chung, H. Claus, M. Kanatzidis, D. Brown, J. Kang, R. Fernandes, I. Eremin, S. Rosenkranz, O. Chmaissem, and R. Osborn, Nature Physics (2016), 10.1038/nphys3629.
  - <sup>14</sup> A. E. Böhmer, F. Hardy, L. Wang, T. Wolf, P. Schweiss, and C. Meingast, Nature Communications **6** (2015), 10.1038/ncomms8911.
  - <sup>15</sup> J. Kang, X. Wang, A. V. Chubukov, and R. M. Fernandes, Physical Review B **91**, 121104 (2015).
  - <sup>16</sup> M. N. Gastiasoro and B. M. Andersen, Physical Review B **92**, 140506 (2015).
  - <sup>17</sup> M. Hoyer, R. M. Fernandes, A. Levchenko, and J. Schmalian, Physical Review B **93**, 144414 (2016).
  - <sup>18</sup> M. H. Christensen, J. Kang, B. M. Andersen, I. Eremin, and R. M. Fernandes, Physical Review B **92**, 214509 (2015).
  - <sup>19</sup> R. M. Fernandes, S. A. Kivelson, and E. Berg, Physical Review B **93**, 014511 (2016).
  - <sup>20</sup> K. M. Taddei, J. M. Allred, D. E. Bugaris, S. Lapidus, M. J. Krogstad, R. Stadel, H. Claus, D. Y. Chung, M. G. Kanatzidis, S. Rosenkranz, R. Osborn, and O. Chmaissem, Physical Review B **93**, 134510 (2016).
  - <sup>21</sup> K. Zhao, Q. Q. Liu, X. C. Wang, Z. Deng, Y. X. Lv, J. L. Zhu, F. Y. Li, and C. Q. Jin, Physical Review B **84**, 184534 (2011).
  - <sup>22</sup> P. Materne, S. Kamusella, R. Sarkar, T. Goltz, J. Spehling, H. Maeter, L. Harnagea, S. Wurmehl, B. Büchner, H. Luetkens, *et al.*, Physical Review B **92**, 134511 (2015).
  - <sup>23</sup> Haberkorn, N. and Maiorov, B. and Jaime, M. and Usov, I. and Miura, M. and Chen, G.F. and Yu, W. and Civale, L., Physical Review B **84** (2011).
  - <sup>24</sup> J. Dong, H. J. Zhang, G. Xu, Z. Li, G. Li, W. Z. Hu, D. Wu, G. F. Chen, X. Dai, J. L. Luo, Z. Fang, and N. L. Wang, EPL (Europhysics Letters) **83**, 27006 (2008).
  - <sup>25</sup> Zhao, K. and Liu, Q.Q. and Wang, X.C. and Deng, Z. and Lv, Y.X. and Zhu, J.L. and Li, F.Y. and Jin, C.Q., Journal of Physics: Condensed Matter **22** (2010).
  - <sup>26</sup> G. Wu, H. Chen, T. Wu, Y. L. Xie, Y. J. Yan, R. H. Liu, X. F. Wang, J. J. Ying, and X. H. Chen, Journal of Physics: Condensed Matter **20**, 422201 (2008).
  - <sup>27</sup> B. H. Toby, Journal of Applied crystallography **34**, 210 (2001).
  - <sup>28</sup> A. C. Larson and R. B. Von Dreele, Report LAUR **86-748** (Los Alamos National Laboratory, Los Alamos, NM, 2004).
  - <sup>29</sup> P. W. Stephens, Journal of Applied Crystallography **32**, 281 (1999).
  - <sup>30</sup> S. Avci, J. M. Allred, O. Chmaissem, D. Y. Chung, S. Rosenkranz, J. A. Schlueter, H. Claus, A. Daoud-Aladine, D. D. Khalyavin, P. Manuel, A. Llobet, M. R. Suchomel, M. G. Kanatzidis, and R. Osborn, Physical Review B **88** (2013), 10.1103/PhysRevB.88.094510.
  - <sup>31</sup> J. M. Allred, S. Avci, D. Y. Chung, H. Claus, D. D. Khalyavin, P. Manuel, K. M. Taddei, M. G. Kanatzidis, S. Rosenkranz, R. Osborn, and O. Chmaissem, Physical Review B **92** (2015), 10.1103/PhysRevB.92.094515.
  - <sup>32</sup> F. Waßer, A. Schneidewind, Y. Sidis, S. Wurmehl, S. Aswartham, B. Büchner, and M. Braden, Physical Review B **91**, 060505 (2015).
  - <sup>33</sup> B. P. P. Mallett, Y. G. Pashkevich, A. Gusev, T. Wolf, and C. Bernhard, EPL (Europhysics Letters) **111**, 57001 (2015).
  - <sup>34</sup> L. Wang, F. Hardy, A. E. Böhmer, T. Wolf, P. Schweiss, and C. Meingast, Physical Review B **93**, 014514 (2016).
  - <sup>35</sup> S. D. Wilson, Z. Yamani, C. R. Rotundu, B. Freelon, E. Bourret-Courchesne, and R. J. Birgeneau, Physical Review B **79**, 184519 (2009).
  - <sup>36</sup> K. Matan, R. Morinaga, K. Iida, and T. J. Sato, Physical Review B **79**, 054526 (2009).
  - <sup>37</sup> S. Avci, O. Chmaissem, D. Y. Chung, S. Rosenkranz, E. A. Goremychkin, J. P. Castellan, I. S. Todorov, J. A. Schlueter, H. Claus, A. Daoud-Aladine, D. D. Khalyavin, M. G. Kanatzidis, and R. Osborn, Physical Review B **85** (2012), 10.1103/PhysRevB.85.184507.
  - <sup>38</sup> B. Saparov, C. Cantoni, M. Pan, T. C. Hogan, W. Ratcliff II, S. D. Wilson, K. Fritsch, B. D. Gaulin, and A. S. Sefat, Scientific reports **4** (2014).
  - <sup>39</sup> K. Kirshenbaum, N. P. Butch, S. R. Saha, P. Y. Zavalij, B. G. Ueland, J. W. Lynn, and J. Paglione, Physical Review B **86**, 060504 (2012).
  - <sup>40</sup> C. Krellner, N. Caroca-Canales, A. Jesche, H. Rosner, A. Ormeci, and C. Geibel, Physical Review B **78**, 100504 (2008).
  - <sup>41</sup> X. Wang, J. Kang, and R. M. Fernandes, Physical Review B **91**, 024401 (2015).
  - <sup>42</sup> R. D. Shannon, Acta Crystallographica Section A: Crystal Physics, Diffraction, Theoretical and General Crystallography **32**, 751 (1976).
  - <sup>43</sup> R. M. Fernandes and J. Schmalian, Superconductor Science and Technology **25**, 084005 (2012).
  - <sup>44</sup> A. Chubukov, M. Khodas, and R. M. Fernandes, arXiv preprint arXiv1602.05503v1 (2016).
  - <sup>45</sup> A. Cano, M. Civelli, I. Eremin, and I. Paul, Physical Review B **82**, 020408 (2010).
  - <sup>46</sup> M. H. Fang, H. M. Pham, B. Qian, T. J. Liu, E. K. Vehstedt, Y. Liu, L. Spinu, and Z. Q. Mao, Physical Review B **78**, 224503 (2008).
  - <sup>47</sup> Lee, C. H. and Iyo, A. and Eisaki, H. and Kito, H. and Fernandez-Diaz, M. T. and Ito, T. and Kihou, K. and Matsuhata, H. and Braden, M. and Yamada, K., Journal of the Physical Society of Japan **77**, 083704 (2008).
  - <sup>48</sup> J. J. Kuchinskii, E. Z. and Nekrasov, I. A. and Sadovskii, M. V., **91**, 518 (2010).
  - <sup>49</sup> H. Usui and K. Kuroki, Physical Review B **84** (2011), 10.1103/PhysRevB.84.024505.
  - <sup>50</sup> Usui, H. and Suzuki, K. and Kazuhiko, K., Superconducting Science and Technology **25** (2012), 10.1088/0953-2048/25/8/084004.
  - <sup>51</sup> T. Miyake, K. Nakamura, R. Arita, and M. Imada, Journal of the Physical Society of Japan **79** (2010), 10.1143/JPSJ.79.044705.